Society of Medical Education & Research

2023, Volume 3, Issue 1, Page No: 104-126
ISSN: 3108-4826

Journal of Medical Sciences and Interdisciplinary Research

Long Noncoding RNA DCST1-AS1 Drives Renal Cell Carcinoma Progression via the miR-582-5p/HMGB2 Axis

Emma Charlotte Green[1]*, Daniel Thomas Wright[1], Julien Philippe Martin[2], Lucas Andre Moreau[2]

[1]Department of Management, University of Exeter Business School, Exeter, United Kingdom.
[2]Department of Management, EM Strasbourg Business School, University of Strasbourg, Strasbourg, France.

***E-mail** ✉ e.green.exeter@gmail.com

Abstract

Accounting for the majority of primary kidney tumors, renal cell carcinoma (RCC) constitutes roughly 80–90% of cases. Despite evidence that long non-coding RNAs (lncRNAs) impact RCC development, their exact mechanisms of action remain largely undefined. RNA sequencing data from 541 renal cell carcinoma (RCC) cases and 71 matched normal adjacent tissues were obtained from the TCGA database. The prognostic significance of the long non-coding RNA DCST1-AS1 in RCC was evaluated through Kaplan-Meier survival analysis, receiver operating characteristic (ROC) curves, and correlations with clinicopathological features. Expression levels of DCST1-AS1 were measured in RCC tissues and cell lines via quantitative real-time PCR. Its subcellular distribution was determined using fluorescence in situ hybridization and nuclear-cytoplasmic fractionation experiments. The biological functions of DCST1-AS1 were explored through various in vitro assays, such as CCK-8 proliferation, colony formation, wound-healing migration, and Transwell invasion/migration tests, along with in vivo studies in RCC xenograft mouse models. Potential interacting partners of DCST1-AS1 were identified using RNA pull-down, luciferase reporter, and RNA immunoprecipitation techniques. The possible activation of the PI3K/AKT/GSK-3β signaling pathway was assessed by Western blotting and immunofluorescence staining. DCST1-AS1 was found to be significantly upregulated in RCC tissues and cell lines, with higher expression correlating with advanced tumor stage, elevated pTNM classification, and poorer patient outcomes. Silencing DCST1-AS1 inhibited RCC cell proliferation, migration, and cell cycle progression, whereas its overexpression accelerated tumor growth and metastatic potential in xenograft mouse models. Mechanistically, DCST1-AS1 acted as a molecular sponge for miR-582-5p, leading to increased HMGB2 expression. In addition, DCST1-AS1 overexpression activated the PI3K/AKT/GSK-3β signaling pathway and promoted nuclear translocation of β-catenin. Functional assays further demonstrated that the PI3K inhibitor LY294002 could partially reverse the oncogenic effects induced by DCST1-AS1 upregulation. DCST1-AS1 contributes to the progression of renal cell carcinoma through regulation of the miR-582-5p/HMGB2 axis, highlighting its potential as a therapeutic target for RCC.

Keywords: Tumorigenesis, Renal cell carcinoma, DCST1-AS1, MiR-582-5p, HMGB2

Introduction

Renal cell carcinoma (RCC) constitutes the majority of primary kidney malignancies, representing roughly 80–90% of cases [1, 2]. Early-stage RCC is often asymptomatic, resulting in late diagnoses when the disease has already progressed. Although surgical interventions, chemotherapy, and targeted therapies have advanced, patient survival remains limited due to recurrence and metastatic spread [2, 3]. This underscores the need to uncover the molecular mechanisms underlying RCC progression and to develop more effective therapeutic approaches.

Within the human genome, protein-coding sequences account for only about 2% of transcriptional regulators,

Access this article online https://smerpub.com/

Received: 12 January 2023; **Accepted:** 11 March 2023

How to cite this article: Green EC, Wright DT, Martin JP, Moreau LA. Long Noncoding RNA DCST1-AS1 Drives Renal Cell Carcinoma Progression via the miR-582-5p/HMGB2 Axis. J Med Sci Interdiscip Res. 2023;3(1):104-26. https://doi.org/10.51847/qKGV9pl7x5

while the majority of regulatory activity is mediated by non-coding RNAs (ncRNAs) [4]. Among these, long non-coding RNAs (lncRNAs), transcripts longer than 200 nucleotides, play critical roles in controlling gene expression and modulating cellular signaling pathways [5]. Aberrant expression of lncRNAs has been implicated in tumorigenesis and cancer progression across a wide range of malignancies [4, 6]. Certain lncRNAs, including lnc-NEF [7], lnc-MAP3K13 [8], and lnc-CTHCC [9], show cancer-specific expression profiles and have emerged as potential biomarkers or therapeutic targets. Beyond gene regulation, lncRNAs can influence tumor growth and metastasis by altering immune evasion and metabolic pathways [10]. A key mode of action for many lncRNAs is functioning as competitive endogenous RNAs (ceRNAs), which sequester microRNAs (miRNAs) and thereby modulate their downstream targets [11, 12]. For instance, LINC00926 promotes RCC progression through a feedback loop involving miR-30a-5p and SOX4 [13], whereas ENTPD3-AS1 inhibits RCC development by binding miR-155-5p and upregulating HIF-1α [14].

DC-STAMP domain-containing 1-antisense 1 (DCST1-AS1) is a newly identified lncRNA that has been reported to be upregulated in various cancers [15, 16]. In endometrial cancer, DCST1-AS1 expression is markedly elevated [17]. Functional studies indicate that its knockdown suppresses hepatocellular carcinoma growth both in vitro and in vivo [18], while in breast cancer, DCST1-AS1 promotes epithelial-mesenchymal transition (EMT) and increases chemoresistance [19]. Across multiple cancer types, higher DCST1-AS1 levels have been associated with tumor size, advanced stage, and resistance to therapy. Nevertheless, the role and clinical significance of DCST1-AS1 in RCC remain unknown.

MiR-582-5p has been reported to regulate high mobility group box 2 (HMGB2) in several disease contexts [20-22], often acting as a tumor suppressor [23, 24]. In clear cell RCC, miR-582-5p inhibits tumor growth by targeting COL5A1 [25]. HMGB2, a regulator of chromatin remodeling and transcription, functions as an oncogene in multiple cancers, and its silencing reduces RCC cell proliferation and invasion [26, 27].

In this study, we identified DCST1-AS1 as a previously uncharacterized lncRNA in RCC and explored its biological function and clinical relevance. We demonstrate that DCST1-AS1 promotes RCC progression via the miR-582-5p/HMGB2 axis and regulates the PI3K/AKT/GSK-3β signaling pathway, suggesting its potential utility as both a biomarker and therapeutic target in RCC.

Materials and Methods

Bioinformatics analysis

RNA sequencing data from 541 renal cell carcinoma (RCC) samples and 71 matched normal tissues were collected from the TCGA database. DCST1-AS1 expression within the TCGA-KIRC cohort was quantified using R software (version 4.3.1). To explore potential regulatory interactions, a competitive endogenous RNA (ceRNA) network was constructed, leveraging the starBase database to identify co-expressed RNAs and candidate target genes. Putative miRNA binding partners of DCST1-AS1 were predicted using LncBase and miRDB, and complementary RNA-RNA interactions were further investigated with TargetScan and starBase.

Clinical samples

A total of 30 pairs of RCC and corresponding normal tissues were obtained from patients undergoing surgery at Taizhou Hospital of Zhejiang Province, affiliated with Wenzhou Medical University (Taizhou, China), all of whom had not received any preoperative adjuvant treatments. The collected specimens were immediately frozen in liquid nitrogen and subsequently stored at −80 °C for later RNA extraction.

Cell culture

Renal cell carcinoma (RCC) cell lines (ACHN, A498, Caki-1, 769-P, 786-O, and SN12C), together with human renal tubular embryonic kidney 293T cells and epithelial HK-2 cells, were obtained from the Cell Bank of the Chinese Academy of Sciences (Shanghai, China). 293T cells were cultured in DMEM (Gibco, Massachusetts, USA) supplemented with 10% fetal bovine serum (FBS) (Gibco) at 37 °C in a humidified incubator with 5% CO_2. The RCC cell lines were maintained under the same conditions in RPMI 1640 medium (Gibco). For experimental treatments, LY294002 (MedChemExpress, #HY-10108, NJ, USA) was added to the culture medium at a working concentration of 10 μg/mL.

Table 1. Association between clinicopathological characteristics and DCST1-AS1 expression levels in RCC patients

Characteristic	Low DCST1-AS1 expression (n=270)	High DCST1-AS1 expression (n=271)	p-value
Age, n (%)			0.065
>60 years	125 (23.1%)	147 (27.2%)	
≤60 years	145 (26.8%)	124 (22.9%)	
Gender, n (%)			0.080
Male	167 (30.9%)	187 (34.6%)	
Female	103 (19.0%)	84 (15.5%)	
Tumor stage, n (%)			0.008
Stage I	151 (28.1%)	122 (22.7%)	
Stage II	30 (5.6%)	29 (5.4%)	
Stage III	61 (11.3%)	62 (11.5%)	
Stage IV	28 (5.2%)	55 (10.2%)	
Pathologic T stage, n (%)			0.008
T1	153 (28.3%)	126 (23.3%)	
T2	35 (6.5%)	36 (6.7%)	
T3	81 (15.0%)	99 (18.3%)	
T4	1 (0.2%)	10 (1.8%)	
Pathologic N stage, n (%)			0.007
N0	129 (50.0%)	113 (43.8%)	
N1	3 (1.2%)	13 (5.0%)	
Pathologic M stage, n (%)			0.003
M0	230 (45.3%)	199 (39.2%)	
M1	28 (5.5%)	51 (10.0%)	
Histologic grade, n (%)			<0.001
G1	7 (1.3%)	7 (1.3%)	
G2	138 (25.9%)	98 (18.4%)	
G3	98 (18.4%)	109 (20.5%)	
G4	22 (4.1%)	54 (10.1%)	

1. Bold indicates statistically significant $p < 0.05$

Lentiviral infection and cell transfection

Lentiviral transfer plasmids incorporating complete sequences for miRNA inhibitors, miRNA mimics, short hairpin RNAs (shRNAs) directed at DCST1-AS1, and overexpression vectors for DCST1-AS1, HMGB2, or combined DCST1-AS1/HMGB2, together with appropriate negative controls, were acquired from GenePharma (Shanghai, China). Cells were transfected employing Lipofectamine 3000 reagent (Invitrogen, USA). Lentiviral particles were prepared according to a prior report [28], encompassing shRNAs named sh1-DCST1-AS1 and sh2-DCST1-AS1 targeting DCST1-AS1, along with a corresponding negative control (sh-NC), as well as lentiviruses designed for HMGB2 or DCST1-AS1 overexpression accompanied by matching empty vector controls. Renal cell carcinoma (RCC) cells underwent infection with these lentiviruses and were then subjected to selection using 2 μg/mL puromycin (Yeason, Shanghai, China) to produce stably expressing cell lines.

Real-time quantitative PCR (RT-qPCR)

Total RNA was purified from cultured cells or tissue specimens utilizing TRIzol reagent (Takara, Tokyo, Japan) in accordance with the manufacturer's guidelines. Complementary DNA (cDNA) was synthesized from the RNA using the PrimeScript™ RT Primer Kit (Takara). Real-time quantitative PCR (qPCR) reactions were executed on the ABI 7500 Sequence Detection System (Applied Biosystems, USA) employing TB Green® Premix (Takara). Expression levels relative to controls were computed via the 2^−ΔΔCt approach, normalizing to GAPDH or U6 as endogenous references

Fluorescent in Situ Hybridization (FISH)

FISH procedures were performed with the RNA FISH SA-Biotin Kit (GenePharma) adhering to the supplied

protocol. Post-hybridization, excess probes were cleared away by repeated washing steps, and cell nuclei were stained using DAPI. Subcellular distribution of DCST1-AS1 was examined under a fluorescence microscope (Zeiss, Germany) fitted with suitable excitation/emission filters.

Nuclear-Cytoplasmic RNA fractionation

The PARIS Kit (Invitrogen) was employed according to the manufacturer's protocol to isolate nuclear and cytoplasmic RNA from the cells. U6 served as a nuclear fractionation control, while GAPDH was used as a cytoplasmic control.

Cell proliferation and clonogenic assays

Cell proliferation was measured using the CCK-8 kit (Biosharp, Beijing, China) per the provided instructions. Briefly, 3×10^3 cells were seeded per well in 96-well plates. At indicated time points, 10 μL CCK-8 reagent was added, followed by incubation for 1 h at 37 °C. Absorbance was recorded at 450 nm on a microplate reader (Thermo Fisher Scientific, USA).

Clonogenic potential was assessed by seeding 8×10^2 cells per 35 mm dish and culturing for 5 days. Dishes were washed twice with PBS, fixed in 4% paraformaldehyde for 15 min, and stained with 0.1% crystal violet for 20 min. Colonies with more than 50 cells were counted and photographed under an inverted microscope (Olympus, Japan).

Transwell assays and wound healing

Migration was evaluated by scratch-wound assay. Cells were grown to ~90% confluence in 6-well plates, and a uniform scratch was made using a 200 μL pipette tip. Loose cells were removed by PBS washing, and the same areas were photographed at 0, 24, and 36 h after wounding.

Invasion capacity was tested using Matrigel-coated Transwell chambers (Corning, NY, USA). A total of 2×10^4 cells in 100 μL serum-free medium were placed in the upper chamber, with 600 μL medium containing 20% FBS in the lower chamber. After 24 h, cells that had traversed the membrane were stained with 0.1% crystal violet and counted/photographed under inverted microscopy.

Flow cytometry

Cell cycle and apoptosis were analyzed using the Cell Cycle and Apoptosis Analysis Kit (BD Biosciences) following the standard protocol. Cells (5×10^5) were fixed overnight in 70% ethanol at 4 °C, washed with PBS, and stained with propidium iodide (PI) in the dark at 37 °C. Phase distribution and apoptotic rates were quantified by flow cytometry (Beckman Coulter, USA).

Transcriptome sequencing

Total RNA was isolated from A498 cells overexpressing DCST1-AS1 and from control cells. Libraries were prepared and sequenced at high depth on the Illumina HiSeq 2000 platform by LC-Bio Technology (Hangzhou, China). Differentially expressed genes were identified with the R package limma using cutoffs of $|\log FC| > 1$ and $p < 0.05$. Associated pathways were explored via KEGG enrichment analysis and gene set enrichment analysis (GSEA).

Dual-luciferase reporter assay

Potential miR-582-5p binding regions in DCST1-AS1 and HMGB2, including wild-type and mutated sequences, were synthesized and inserted into pmirGLO vectors (GENEWIZ, Nanjing, China). Cells were co-transfected with these reporter constructs and miR-582-5p mimics. Luciferase activity was detected using the Luciferase Reporter Assay Kit (MeilunBio, Dalian, China) per the protocol, with firefly luciferase signals normalized against Renilla luciferase.

Western blotting

Cells and tissues were homogenized in RIPA lysis buffer containing protease and phosphatase inhibitors (Beyotime, Beijing, China). Protein levels were measured via BCA assay. Samples were separated on 10% SDS-PAGE gels and blotted onto PVDF membranes (Millipore, CA, USA). Following blocking, membranes were probed overnight at 4 °C with primary antibodies targeting AKT (#4685, CST, USA), p-AKT (#4060, CST), PI3K (#4292, CST), p-PI3K (#17366, CST), β-catenin (#GTX633010, GeneTex, China), p-β-catenin (#9566, CST), p-GSK-3β (#9322, CST), Cyclin D1 (#2978, CST), CDK2 (#CY5020, Abways Technology, China), CDK4 (#CY5836, Abways Technology), p21 (#2947, CST), E-cadherin (#GTX100443, GeneTex), N-cadherin (#13116, CST), vimentin (#5741, CST), HMGB2 (#HA721925, HUABIO, Hangzhou, China), and β-actin (#4970, CST). Membranes were then incubated with HRP-conjugated secondary antibodies for 2 h at room temperature, and signals were detected via enhanced chemiluminescence

(Millipore). β-actin was used as the loading control, and densitometry was performed with ImageJ (version 1.0).

Immunofluorescent staining

Cells were fixed in 4% paraformaldehyde for 15 min, permeabilized with 0.1% Triton X-100 for 20 min, and incubated with anti-β-catenin antibody overnight at 4 °C. After PBS rinsing, cells were treated with Cy3-labeled secondary antibody for 1 h at room temperature. Nuclei were stained with DAPI for 10 min, and fluorescence images were acquired.

Biotin-miRNA pull-down

Wild-type and mutant biotinylated miR-582-5p, along with a control, were synthesized by GenePharma and introduced into cells via transfection for 48 h. Lysates were prepared and incubated overnight at 4 °C with streptavidin magnetic beads (Yeason). Beads underwent three washes in cold lysis buffer followed by one in high-salt buffer (0.1% SDS, 1% Triton X-100, 2 mM EDTA, 500 mM NaCl, 20 mM Tris-HCl, pH 8.0). Captured RNA was isolated with TRIzol and detected by qPCR.

RIP assay

Binding of miR-582-5p to DCST1-AS1 and Ago2 was assessed using the BeyoRIP Kit (Beyotime) according to instructions. Precipitated RNA was purified and measured by qPCR, normalized to input controls.

Animal experiment

Male BALB/c nude mice (4 weeks old) were purchased from SLAC Experimental Animal Co., Ltd. (Shanghai, China). For tumor growth experiments, mice were divided randomly into three groups (n = 5 each), and 3 × 10^6 cells in 100 µL PBS were injected subcutaneously into the right flank. Tumor sizes were recorded every two days using calipers, with volumes calculated as 1/2 × length × width^2. At day 34 post-implantation, mice were sacrificed, and excised tumors were weighed.

In the metastasis model, mice were grouped similarly (n = 5), and 2 × 10^6 cells in 100 µL PBS were delivered via tail vein. After 8 weeks, lungs were examined for metastatic foci following euthanasia. In vivo imaging was performed with the IVIS Lumina system (PerkinElmer, USA). Tumor samples were processed for H&E staining and IHC as previously described [28].

Statistical methods

All analyses were conducted with GraphPad Prism (version 9.0). Relationships between DCST1-AS1 expression and clinicopathological features in renal cell carcinoma (RCC) patients were examined using chi-square tests. Kaplan-Meier plots were constructed for survival analysis, and group differences were evaluated with log-rank tests. The prognostic relevance of DCST1-AS1 was investigated through Cox proportional hazards models. Gene expression correlations were determined via Pearson's correlation coefficient. Two-group comparisons employed unpaired Student's t-tests, whereas comparisons across multiple groups used one-way analysis of variance (ANOVA). All values are expressed as mean ± standard deviation (SD) based on triplicate independent experiments. A threshold of $P < 0.05$ denoted statistical significance.

Findings

Overexpression of DCST1-AS1 in RCC tumors and cell lines

Review of RNA-sequencing data from the TCGA-KIRC database showed substantial overexpression of DCST1-AS1 in RCC tumors compared with non-cancerous tissues ($p < 0.001$) **(Figure 1a).** This elevation was more evident in higher-grade tumors and those with distant metastatic spread **(Figures 1b–c).** Survival analysis via Kaplan-Meier method revealed that increased DCST1-AS1 expression strongly predicted worse overall survival (OS) ($p < 0.001$) **(Figure 1d)**, progression-free interval (PFI) ($p = 0.001$)**,** and disease-specific survival (DSS) ($p < 0.001$)**,** with patients in the low-expression group exhibiting extended survival times. Evaluation of clinicopathological variables demonstrated significant correlations between higher DCST1-AS1 and advanced tumor stage ($p = 0.008$), T stage ($p = 0.008$), N stage ($p = 0.007$), metastatic recurrence ($p = 0.003$), and higher histological grade ($p < 0.001$) **(Table 1).** Assessment via receiver operating characteristic (ROC) curves highlighted robust diagnostic utility of DCST1-AS1 for distinguishing RCC (AUC = 0.895). Both univariate and multivariate Cox analyses confirmed DCST1-AS1 as an independent predictor of prognosis in RCC (hazard ratio [HR] = 2.272, $p < 0.001$).

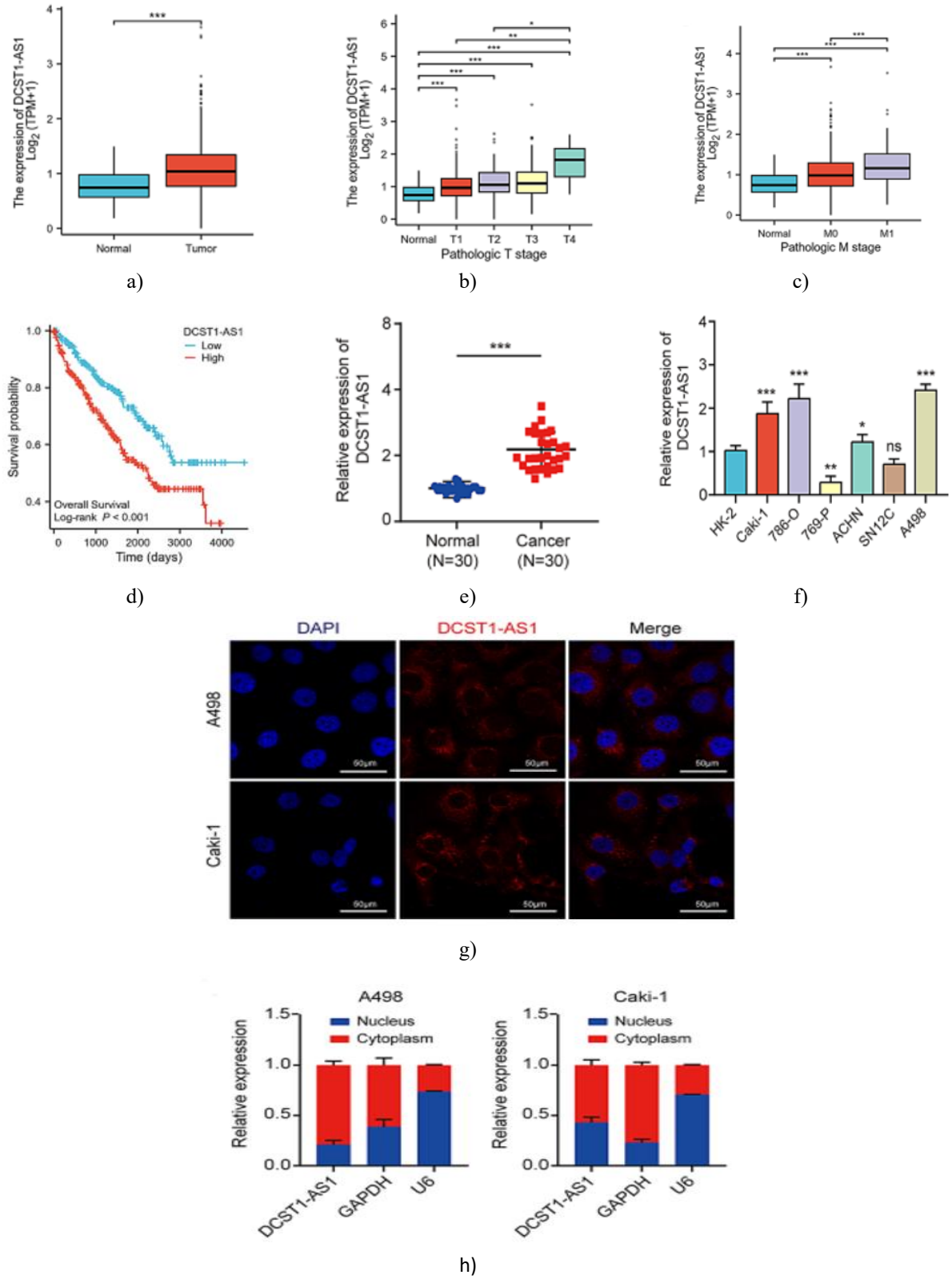

Figure 1. DCST1-AS1 is overexpressed in RCC and predominantly localized in the cytoplasm. (a) Analysis of TCGA data demonstrated significantly higher DCST1-AS1 expression in RCC tissues compared with adjacent non-tumorous samples. (b, c) Increased DCST1-AS1 expression was positively associated with advanced

pathological T stage and the presence of distant metastasis. (d) Kaplan–Meier survival analysis revealed that patients with high DCST1-AS1 expression exhibited significantly poorer overall survival. (e) qPCR validation in 30 paired clinical specimens confirmed elevated DCST1-AS1 levels in RCC tissues. (f) Compared with the normal renal epithelial cell line HK-2, most RCC cell lines displayed increased DCST1-AS1 expression, with the exception of 769-P cells. (g) Fluorescence in situ hybridization showed that DCST1-AS1 was mainly distributed in the cytoplasm of A498 and Caki-1 cells. (h) Nuclear–cytoplasmic fractionation further verified the cytoplasmic predominance of DCST1-AS1. Data are presented as mean ± SD from three independent experiments.

Evaluation of DCST1-AS1 expression in clinical samples revealed a pronounced increase in RCC tissues relative to paired normal kidney tissues. Similar expression patterns were observed in RCC-derived cell lines, in which DCST1-AS1 levels were generally higher than those in HK-2 cells. Notably, fluorescence-based localization and biochemical fractionation approaches consistently indicated that DCST1-AS1 resides primarily in the cytoplasmic compartment of RCC cells, suggesting a potential post-transcriptional regulatory function.

Silencing DCST1-AS1 restrains RCC cell growth through disruption of G1/S transition

In light of the association between DCST1-AS1 abundance and aggressive clinicopathological features, we explored its biological role in RCC progression. Efficient depletion of DCST1-AS1 was achieved in multiple RCC cell lines, while ectopic expression was established in selected models. Functional assays revealed that loss of DCST1-AS1 markedly impaired proliferative capacity in A498 and Caki-1 cells. Cell cycle profiling demonstrated that DCST1-AS1 suppression led to a pronounced accumulation of cells in the G1 phase, accompanied by a reduction in S phase entry. Consistent with these observations, key regulators of G1/S progression were dysregulated following DCST1-AS1 knockdown, as evidenced by decreased expression of Cyclin D1, CDK2, and CDK4 and concomitant upregulation of the cell cycle inhibitor p21. Together, these findings indicate that DCST1-AS1 facilitates RCC cell proliferation by promoting G1/S phase progression.

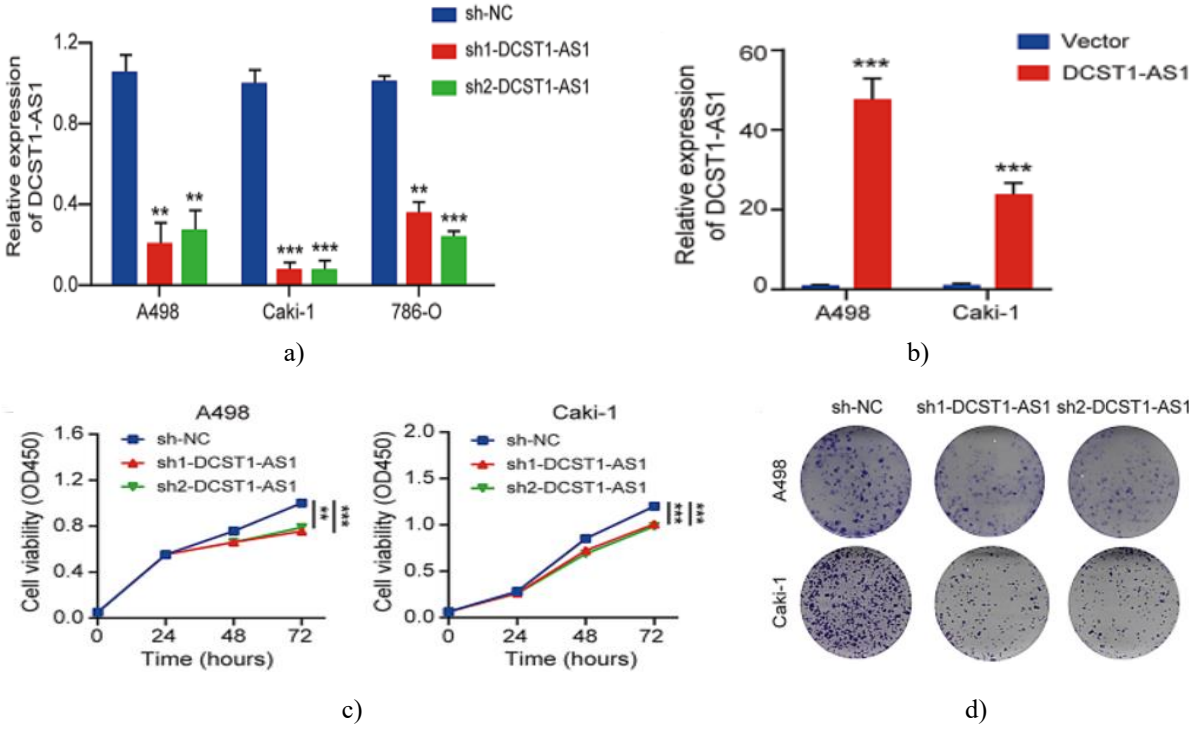

a) b)

c) d)

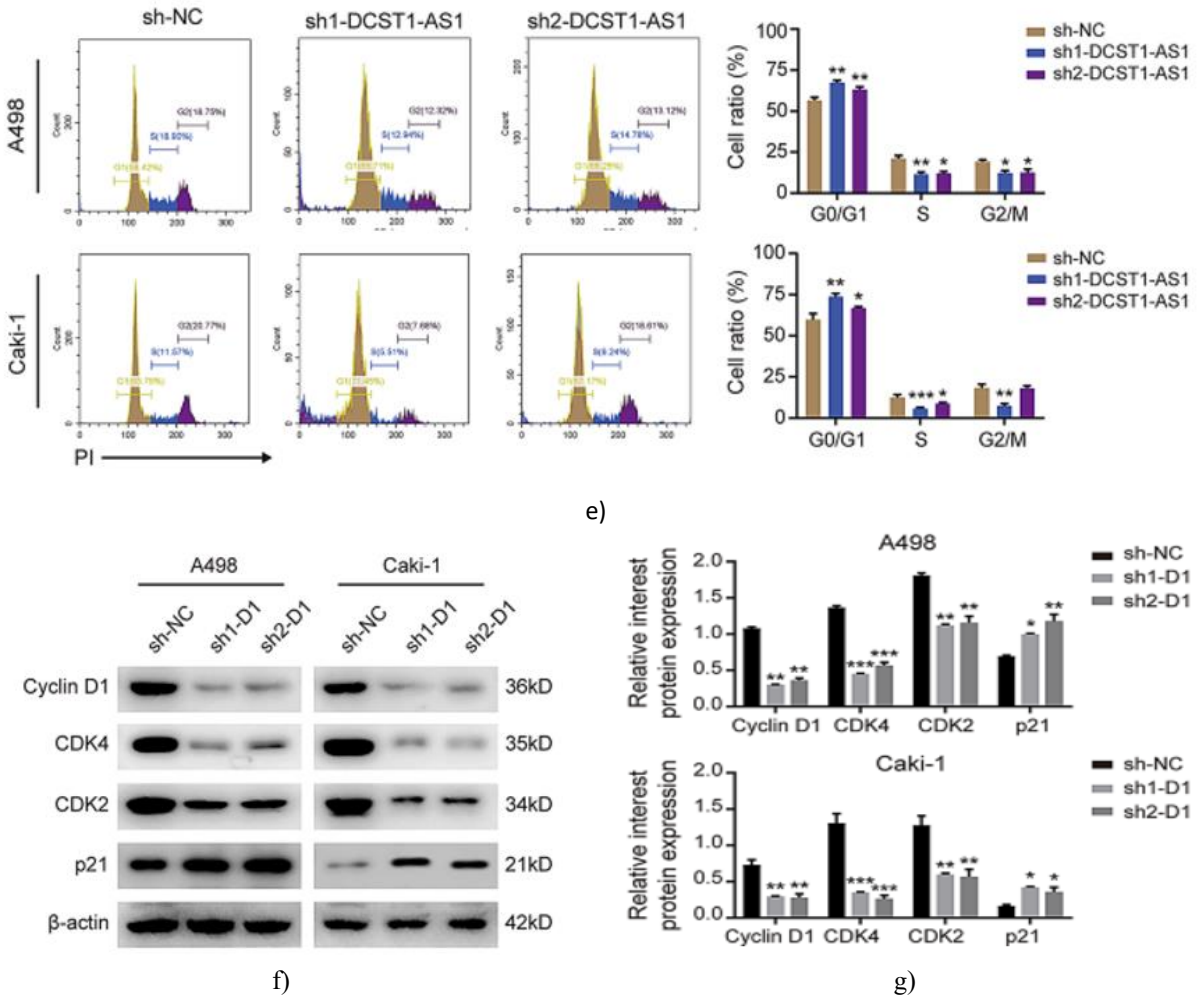

Figure 2. Reduction of DCST1-AS1 impairs proliferative capacity and halts cell cycle advancement in RCC cells. a**.** Quantitative PCR confirming efficient suppression of DCST1-AS1 in A498, Caki-1, and 786-O cells following infection with sh-DCST1-AS1 lentivirus relative to sh-NC controls. b. Verification of enforced DCST1-AS1 expression in A498 and Caki-1 cells transduced with DCST1-AS1–encoding lentivirus compared with empty vector. c**.** CCK-8 analysis demonstrating diminished metabolic activity in A498 and Caki-1 cells after DCST1-AS1 silencing. d**.** Clonogenic assays revealing a substantial decrease in long-term colony-forming ability upon DCST1-AS1 knockdown. e. Flow cytometry profiles showing accumulation of cells in the G1 phase and reduced entry into S phase following DCST1-AS1 depletion. f**.** Immunoblot analysis illustrating altered expression of G1/S checkpoint regulators, including downregulation of Cyclin D1, CDK2, and CDK4 and upregulation of p21. g. Densitometric analysis of immunoblot bands normalized to loading controls. Values represent mean ± SD from three independent experiments. $p < 0.05$; $p < 0.01$; $p < 0.001$ (Student's t-test or one-way ANOVA).

Loss of DCST1-AS1 limits RCC cell motility and invasive behavior

To determine whether DCST1-AS1 influences the metastatic phenotype of RCC cells, functional motility assays were performed. Invasion assays conducted using Matrigel-coated Transwell chambers revealed a pronounced decline in the number of invading cells following DCST1-AS1 knockdown **(Figures 3a–b).** Consistent with these findings, scratch wound closure occurred at a markedly slower rate in DCST1-AS1–deficient cells than in control cells **(Figure 3c).** At the molecular level, depletion of DCST1-AS1 shifted the expression pattern of epithelial–mesenchymal transition markers, characterized by enhanced E-cadherin

expression and concomitant reductions in N-cadherin and vimentin **(Figures 3d–e)**. These results indicate that DCST1-AS1 contributes to the acquisition of migratory and invasive properties in RCC cells.

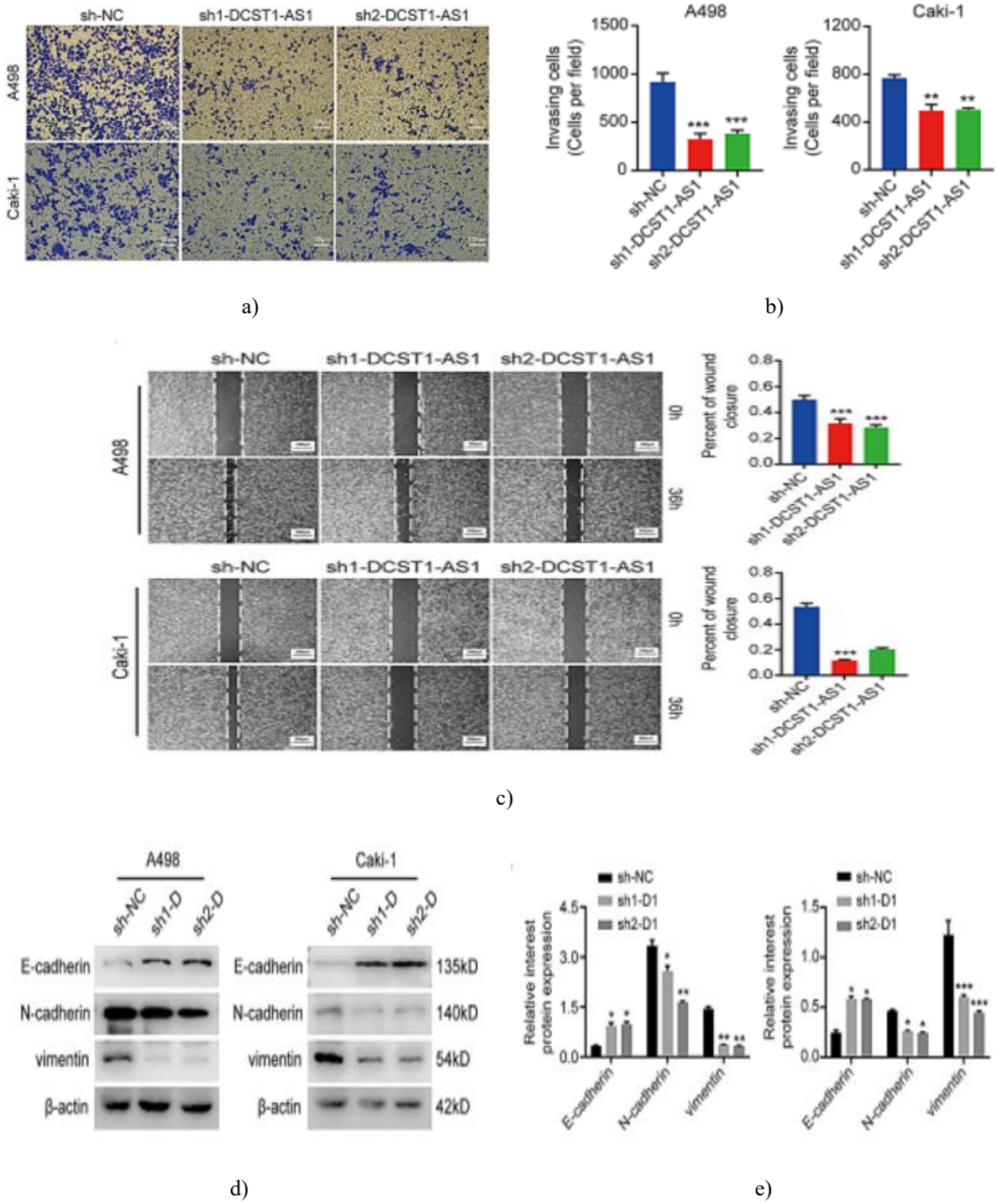

Figure 3. Silencing DCST1-AS1 diminishes migratory and invasive properties of RCC cells. a**.** Representative images from Transwell invasion assays showing reduced invasiveness of A498 and Caki-1 cells following DCST1-AS1 knockdown. Scale bar = 100 μm. b**.** Statistical analysis of invaded cell numbers corresponding to

panel A. **C.** Wound-healing assays illustrating impaired migratory capacity of DCST1-AS1–deficient A498 and Caki-1 cells. Scale bar = 500 μm. **d.** Immunoblot analysis of epithelial–mesenchymal transition–associated proteins, including E-cadherin, N-cadherin, and vimentin, in A498 and Caki-1 cells after DCST1-AS1 suppression. **e.** Densitometric quantification of protein expression levels shown in panel D. Data represent mean ± SD from three independent experiments. $p < 0.05$; $p < 0.01$; $p < 0.001$ (Student's t-test or one-way ANOVA).

DCST1-AS1 acts as a competing endogenous RNA by sequestering miR-582-5p in RCC cells

Given its predominant cytoplasmic localization, DCST1-AS1 was hypothesized to participate in post-transcriptional regulation through interaction with microRNAs. To investigate this possibility, transcriptome-wide miRNA profiling was performed in A498 cells overexpressing DCST1-AS1 and corresponding control cells **(Figures 4a).** Differential expression analysis identified 61 miRNAs with increased expression and 59 miRNAs with decreased expression ($|logFC| > 1.5$, $p < 0.01$; **Figure 4b**).

To narrow down potential miRNAs directly regulated by DCST1-AS1, predicted binding partners were screened using the LncBase and miRDB databases. Integration of bioinformatic predictions with RNA-sequencing data revealed three overlapping candidate miRNAs—miR-6516-5p, miR-582-5p, and miR-4797-5p—as illustrated in the Venn diagram **(Figure 4c).** Direct binding between DCST1-AS1 and these candidates was then evaluated using dual-luciferase reporter assays in 293T cells. Among the tested miRNAs, only miR-582-5p significantly suppressed luciferase activity **(Figure 4d),** indicating a specific interaction.

Subsequent transfection of miR-582-5p mimics into A498 and 786-O cells confirmed effective overexpression **(Figure 4e).** Luciferase reporter assays further demonstrated that miR-582-5p markedly reduced reporter activity driven by wild-type DCST1-AS1, whereas mutation of the predicted binding site abolished this effect **(Figure 4f).** These findings establish DCST1-AS1 as a molecular sponge for miR-582-5p in RCC cells.

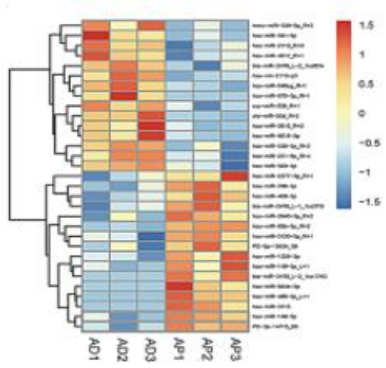

a)

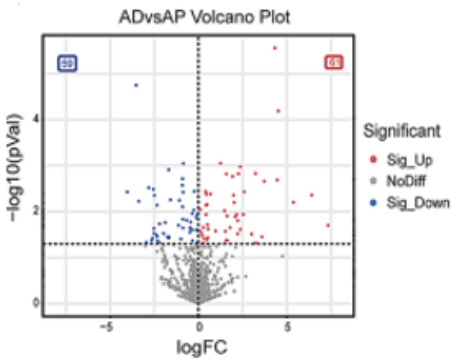

b)

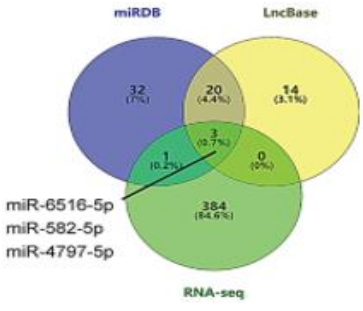

c)

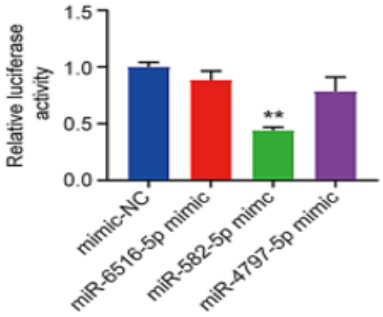

d)

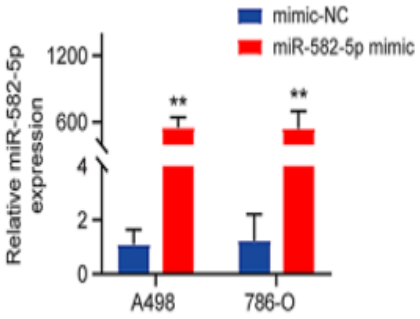
mimic-NC
miR-582-5p mimic
Relative miR-582-5p expression
1200
600
4
2
0
**
**
A498
786-O

e)

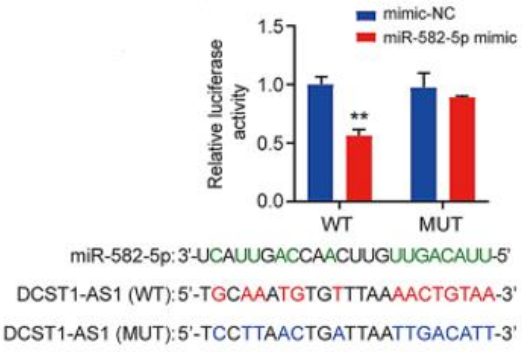
mimic-NC
miR-582-5p mimic
Relative luciferase activity
1.5
1.0
0.5
0.0
**
WT
MUT
miR-582-5p: 3'-UCAUUGACCAACUUGUUGACAUU-5'
DCST1-AS1 (WT): 5'-TGCAAATGTGTTTAAAACTGTAA-3'
DCST1-AS1 (MUT): 5'-TCCTTAACTGATTAATTGACATT-3'

f)

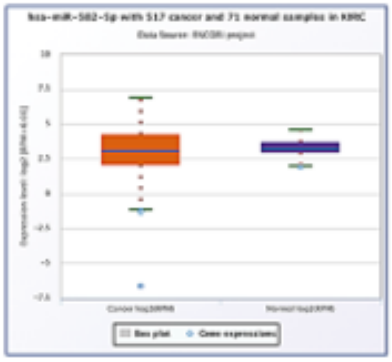

g)

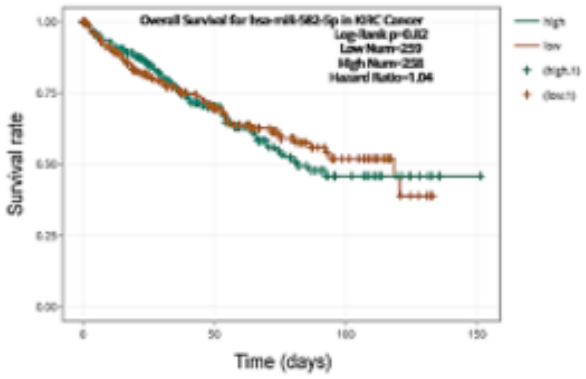
Survival rate
Time (days)
high
low

h)

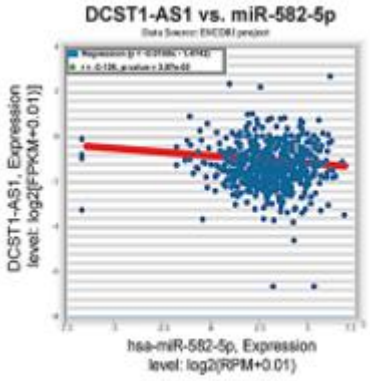
DCST1-AS1 vs. miR-582-5p
DCST1-AS1, Expression level: log2[FPKM+0.01)]
hsa-miR-582-5p, Expression level: log2(RPM+0.01)

i)

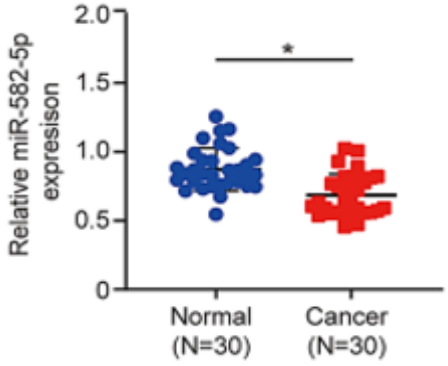
Relative miR-582-5p expresison
2.0
1.5
1.0
0.5
0
*
Normal (N=30)
Cancer (N=30)

j)

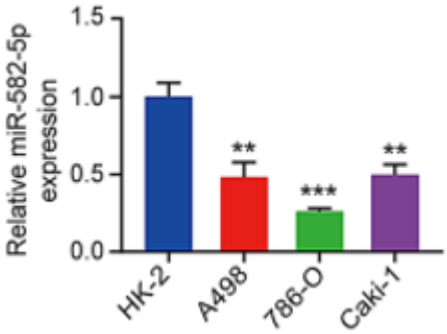
Relative miR-582-5p expression
1.5
1.0
0.5
0.0
**
***
**
HK-2
A498
786-O
Caki-1

k)

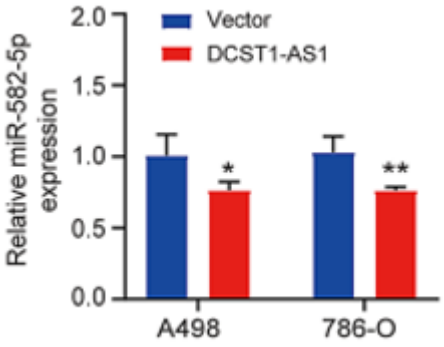
Vector
DCST1-AS1
Relative miR-582-5p expression
2.0
1.5
1.0
0.5
0.0
*
**
A498
786-O

l)

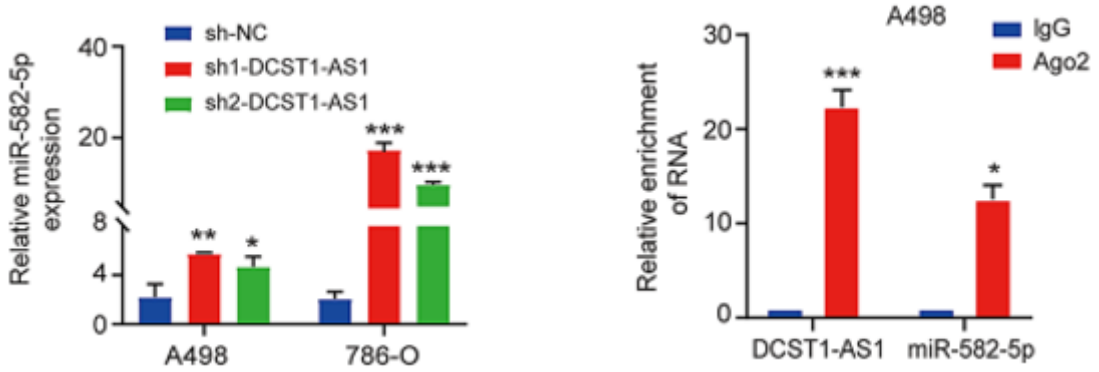

Figure 4. DCST1-AS1 acts as a competing endogenous RNA for miR-582-5p in RCC cells**.** **A.** Heatmap illustrating global miRNA expression changes in DCST1-AS1–overexpressing A498 cells compared with control cells. **B.** Volcano plot depicting significantly dysregulated miRNAs following DCST1-AS1 overexpression; red and blue points represent upregulated and downregulated miRNAs, respectively (|logFC| > 1.5, $P < 0.01$). **C.** Venn diagram showing intersecting miRNAs predicted to bind DCST1-AS1 based on LncBase, miRDB, and RNA-seq datasets. **D.** Dual-luciferase reporter assay results in 293T cells co-transfected with wild-type DCST1-AS1 reporter constructs and individual miRNA mimics (miR-6516-5p, miR-582-5p, miR-4797-5p) or negative control. **E.** qPCR validation of miR-582-5p overexpression in A498 and 786-O cells following transfection with miR-582-5p mimics. **F.** Luciferase reporter analysis in A498 cells co-transfected with miR-582-5p mimics and wild-type or mutant DCST1-AS1 reporters; schematic alignment of miR-582-5p binding sites within DCST1-AS1 is shown. **G.** miR-582-5p expression levels in RCC and normal kidney tissues obtained from starBase (517 tumors vs. 71 normal samples; $p = 0.026$, Student's *t*-test). **H.** Kaplan–Meier survival curves illustrating overall survival stratified by miR-582-5p expression in RCC patients from starBase ($p = 0.0037$; log-rank test).**I.** Pearson correlation analysis demonstrating an inverse relationship between miR-582-5p and DCST1-AS1 expression in RCC tissues ($r = -0.126$, $p = 0.0307$). **J.** qPCR assessment of miR-582-5p levels in 30 matched RCC and adjacent non-tumorous tissue samples. **K.** Expression of miR-582-5p in RCC cell lines (A498, Caki-1, and 786-O) compared with normal renal epithelial HK-2 cells. **L, M.** miR-582-5p expression changes in A498 and 786-O cells following DCST1-AS1 overexpression (**L**) or silencing (**M**). **N.** RNA immunoprecipitation assays using anti-Ago2 antibodies in A498 cells transfected with miR-582-5p mimics, followed by qPCR detection of DCST1-AS1 and miR-582-5p. **O.** RNA pull-down assays showing enrichment of DCST1-AS1 after capture with biotin-labeled wild-type miR-582-5p compared with mutant probes; a nonspecific probe served as a negative control. Data are presented as mean ± SD from three independent experiments. $p < 0.05$; **p** < 0.01; **p** < 0.001 (Student's *t*-test or one-way ANOVA).

Independent validation using starBase datasets confirmed that miR-582-5p expression was significantly reduced in RCC tissues and that higher miR-582-5p levels were associated with improved patient survival **(Figures 4g–h).** Correlation analysis further revealed an inverse association between miR-582-5p and DCST1-AS1 expression **(Figure 4i).** These findings were corroborated by qPCR analysis of clinical specimens, which demonstrated lower miR-582-5p expression in RCC tissues compared with matched normal samples **(Figure 4j).** Similarly, RCC cell lines exhibited decreased miR-582-5p levels relative to HK-2 cells **(Figure 4k).** Manipulation of DCST1-AS1 expression revealed reciprocal regulation of miR-582-5p, as enforced DCST1-AS1 expression suppressed miR-582-5p levels, whereas DCST1-AS1 depletion led to miR-582-5p upregulation **(Figures 4l–m).**

Given the role of Ago2 in miRNA-mediated gene silencing, RIP assays were performed in A498 cells. These experiments demonstrated enhanced enrichment of both DCST1-AS1 and miR-582-5p within Ago2-containing complexes **(Figure 4n).** RNA pull-down assays further verified direct interaction between DCST1-AS1 and miR-582-5p, as DCST1-AS1 was preferentially captured by biotin-labeled wild-type miR-582-5p probes **(Figure 4o).** Functional rescue assays showed that restoration of miR-582-5p partially reversed the suppressive effects of DCST1-AS1 knockdown on RCC cell proliferation and migration **(Figures S2a–d).** Together, these data support a model in which DCST1-AS1 functions as a molecular sponge for miR-582-5p in RCC.

DCST1-AS1 enhances RCC cell proliferation and metastasis through regulation of HMGB2

To identify downstream effectors of the DCST1-AS1/miR-582-5p axis, differential gene expression analysis was performed in DCST1-AS1–overexpressing A498 cells. The top 20 genes exhibiting the most pronounced expression changes are shown in the volcano plot **(Figure 5a).** Among these candidates, HMGB2 emerged as a clinically relevant target. Analysis of starBase datasets revealed that HMGB2 was significantly upregulated in RCC tissues and that elevated HMGB2 expression correlated with unfavorable overall survival. Co-expression analyses demonstrated that RCC samples with high DCST1-AS1 expression displayed concomitant suppression of miR-582-5p and increased HMGB2 levels, suggesting the presence of a ceRNA regulatory network.

qPCR validation confirmed elevated HMGB2 expression in RCC tissues **(Figure 5b).** Direct targeting of HMGB2 by miR-582-5p was established through luciferase reporter assays **(Figure 5c),** while Ago2 RIP assays showed enhanced enrichment of HMGB2 transcripts in miR-582-5p–overexpressing A498 cells **(Figure 5d).** Consistently, DCST1-AS1 knockdown reduced HMGB2 protein expression, an effect that was reversed by miR-582-5p inhibition in both A498 and 786-O cells.

To determine whether HMGB2 mediates the oncogenic effects of DCST1-AS1, rescue experiments were performed using HMGB2-overexpressing lentivirus in DCST1-AS1–silenced cells **(Figures 5e–f).** Restoration of HMGB2 expression effectively rescued the impaired proliferative, migratory, and invasive capacities induced by DCST1-AS1 depletion **(Figures 5g–k).** Collectively, these findings demonstrate that DCST1-AS1 promotes RCC progression by modulating the miR-582-5p/HMGB2 signaling axis.

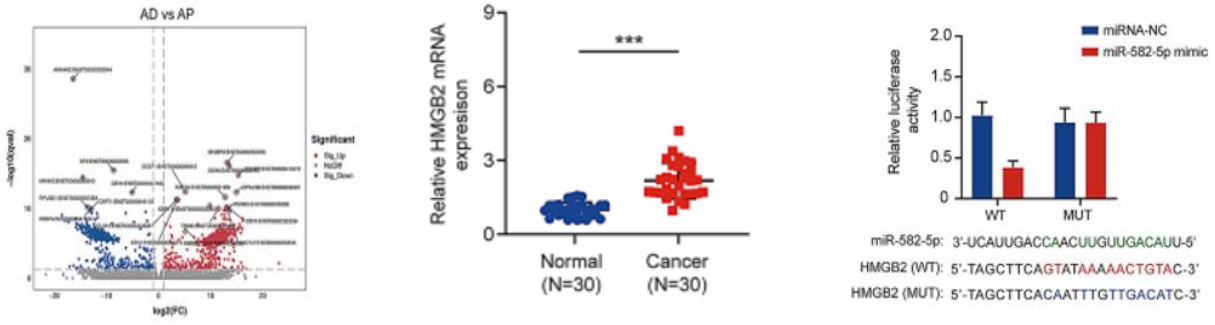

a) b) c)

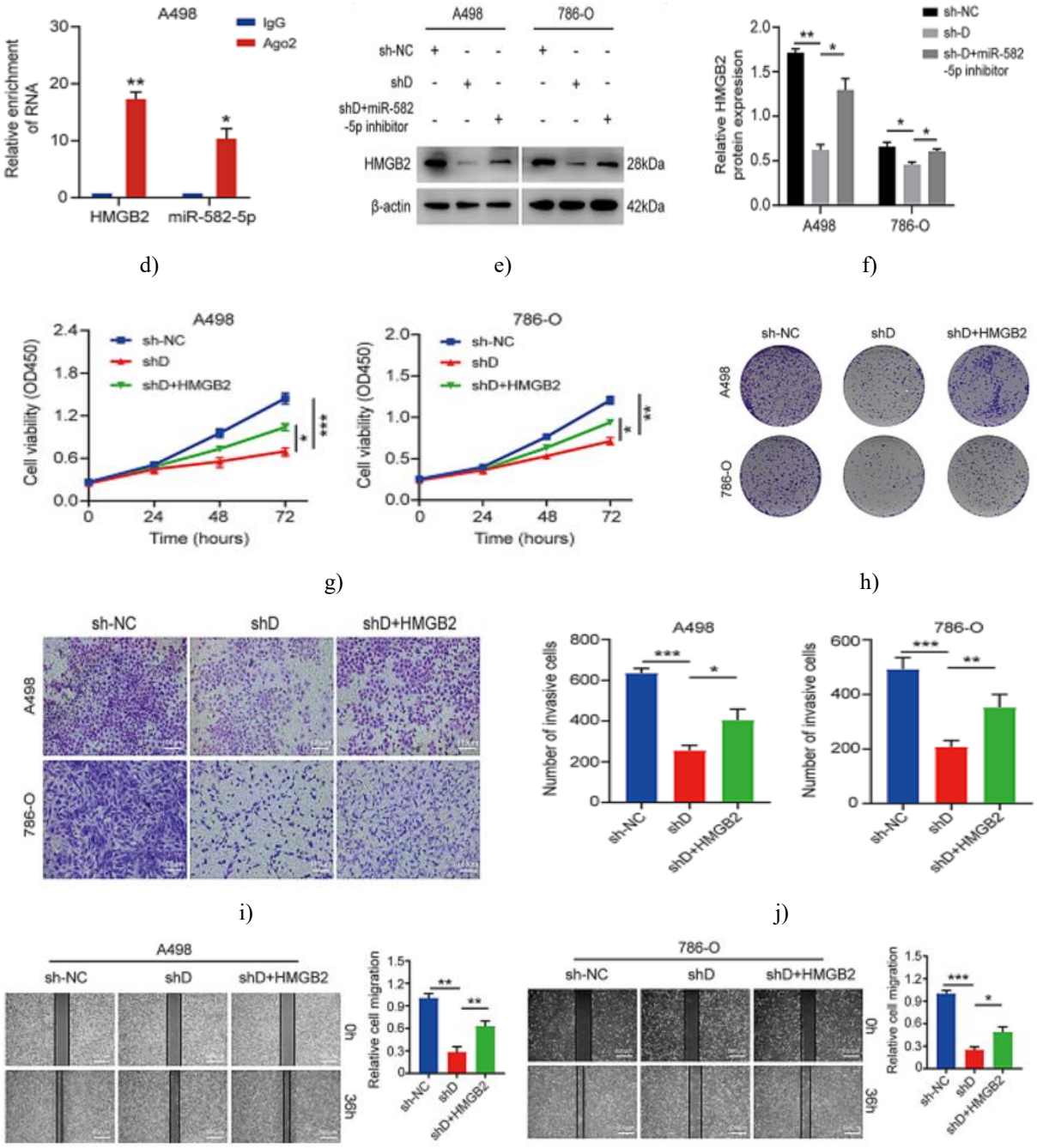

Figure 5. DCST1-AS1 elevates HMGB2 expression through sequestration of miR-582-5p. a**.** Volcano plot illustrating genes differentially expressed between A498 cells overexpressing DCST1-AS1 and corresponding control cells; red and blue points denote significantly upregulated and downregulated transcripts, respectively (|logFC| > 1.5, P < 0.01). b. qPCR analysis of HMGB2 expression in 30 matched RCC and adjacent normal tissue samples. c**.** Dual-luciferase reporter assays performed in A498 cells co-transfected with HMGB2 3′UTR reporter constructs and either miR-582-5p inhibitors or negative control oligonucleotides; predicted binding sites between miR-582-5p and the HMGB2 3′UTR are shown. d. RNA immunoprecipitation using anti-Ago2 antibodies in A498 cells transiently overexpressing miR-582-5p, followed by qPCR quantification of HMGB2 and miR-582-5p

enrichment. e. Western blot analysis of HMGB2 expression in A498 and 786-O cells infected with control lentivirus (sh-NC) or DCST1-AS1–targeting lentivirus (sh1-DCST1-AS1), with or without co-treatment with miR-582-5p inhibitor. f. Densitometric quantification of protein bands shown in panel E. g–k. Functional assays evaluating cellular behavior, including proliferation assessed by CCK-8 (g), clonogenic potential (h), invasive capacity measured by Transwell assays (i, j), and migratory ability assessed by wound-healing assays (k). Data are presented as mean ± SD from three independent experiments. $p < 0.05$; **p** < 0.01; **p** < 0.001 (Student's t-test or one-way ANOVA).

DCST1-AS1 enhances RCC tumor growth and metastatic potential in vivo

To assess the oncogenic role of DCST1-AS1 in vivo, equal numbers of A498 cells from three groups—unmodified parental cells (A498/Control), vector-transduced cells expressing GFP (A498/Vector), and cells stably overexpressing DCST1-AS1 (A498/DCST1-AS1)—were subcutaneously implanted into the flanks of nude mice (n = 5 per group). After 34 days, tumors were excised for evaluation. Both tumor volume and tumor weight were significantly increased in mice injected with A498/DCST1-AS1 cells compared with those receiving A498/Control or A498/Vector cells **(Figures 6a–b).** No overt metastatic lesions were detected in the liver or lungs of mice from any group **(Figure 6c).**

Longitudinal monitoring revealed that tumor growth rates were comparable between the control and vector groups, whereas tumors derived from DCST1-AS1–overexpressing cells exhibited accelerated growth **(Figures 6d).** Throughout the experimental period, no significant differences in body weight were observed among the groups, indicating minimal systemic toxicity **(Figure 6e).** Molecular analyses of excised tumors demonstrated elevated expression of DCST1-AS1 and HMGB2, accompanied by reduced miR-582-5p levels in the DCST1-AS1–overexpressing group **(Figures 6f–h).** Immunohistochemical staining further showed increased Ki-67 and HMGB2 positivity in tumors from the A498/DCST1-AS1 group relative to vector controls, supporting the involvement of the DCST1-AS1/miR-582-5p/HMGB2 axis in RCC tumor progression in vivo **(Figures 6i–j).**

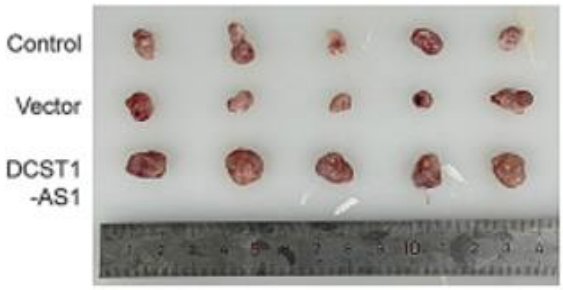

a)

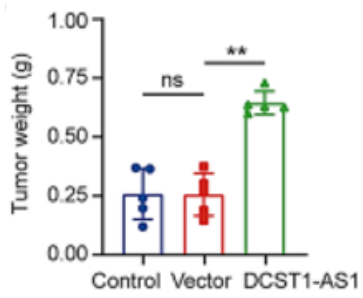

b)

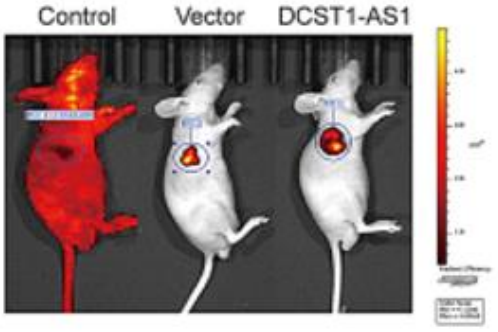

c)

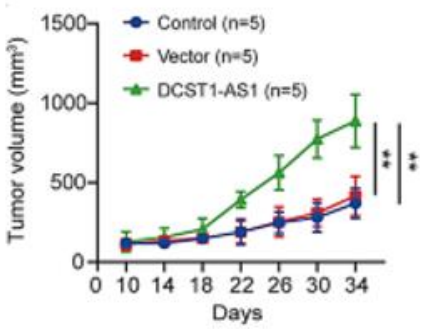

d)

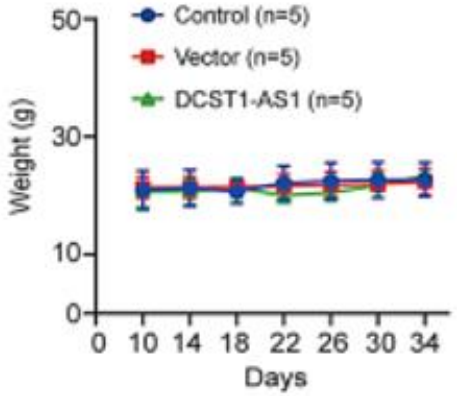
Control (n=5)
Vector (n=5)
DCST1-AS1 (n=5)
Weight (g)
50
30
10
0
0 10 14 18 22 26 30 34
Days

e)

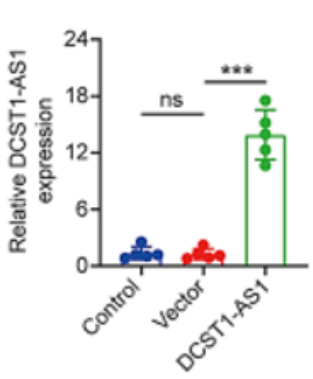
Relative DCST1-AS1 expression
24
18
12
6
0
ns
***
Control
Vector
DCST1-AS1

f)

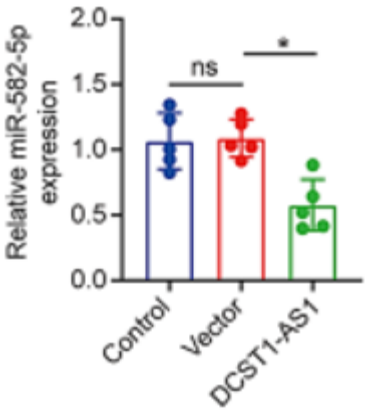
Relative miR-582-5p expression
2.0
1.5
1.0
0.5
0.0
ns
*
Control
Vector
DCST1-AS1

g)

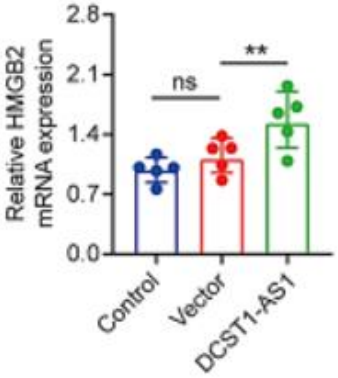
Relative HMGB2 mRNA expression
2.8
2.1
1.4
0.7
0.0
ns
**
Control
Vector
DCST1-AS1

h)

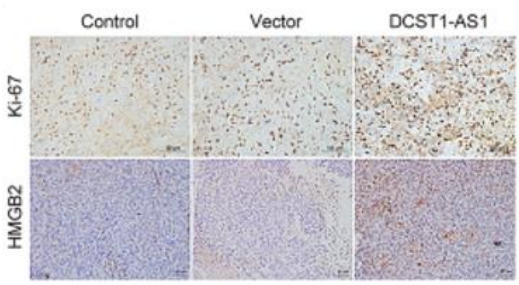
Control
Vector
DCST1-AS1
Ki-67
HMGB2

i)

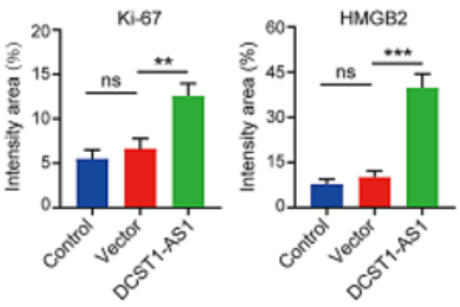
Ki-67
Intensity area (%)
20
15
10
5
0
ns
**
Control
Vector
DCST1-AS1
HMGB2
Intensity area (%)
60
45
30
15
0
ns
***
Control
Vector
DCST1-AS1

j)

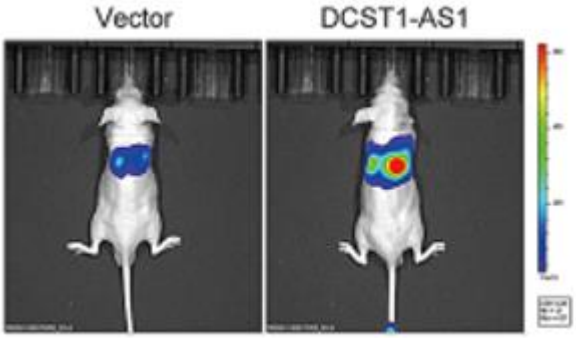
Vector
DCST1-AS1

k)

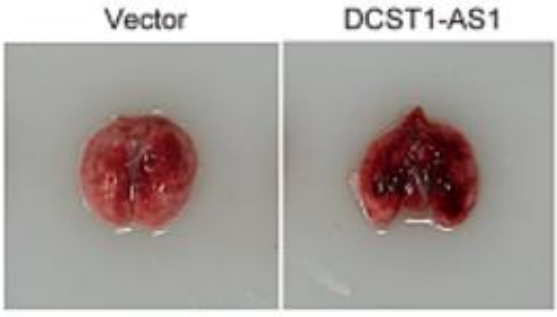
Vector
DCST1-AS1

l)

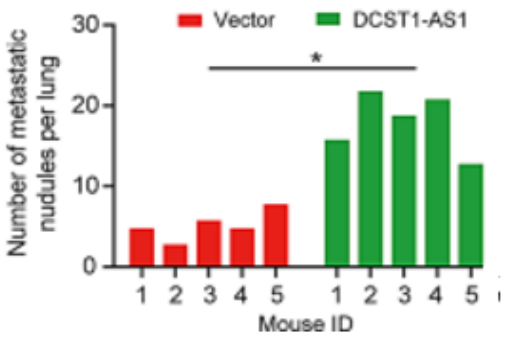

m)

Figure 6. DCST1-AS1 enhances RCC tumor formation and metastatic dissemination in vivo. **a.** Representative images of excised tumor masses obtained from xenograft-bearing mice. **b.** Comparison of tumor weights among different experimental groups. **c.** Representative fluorescence imaging of xenograft tumors in mice. **d.** Tumor growth kinetics measured over the experimental period. **e.** Changes in body weight of mice during tumor development. f–h**.** qPCR analysis of DCST1-AS1 (**f**), miR-582-5p (**g**), and HMGB2 (**h**) expression in excised tumor tissues. **i.** Representative immunohistochemical staining images of Ki-67 and HMGB2 in tumor sections. Ki-67 and HMGB2 are shown in blue and are predominantly nuclear, whereas cytoplasmic regions are stained brown. Scale bar = 100 μm. **j.** Quantitative analysis of Ki-67– and HMGB2–positive staining. **k.** Representative bioluminescent images of metastatic tumor foci in vivo. **l.** Gross images of lung tissues showing metastatic nodules in mice (n = 5 per group). **m.** Statistical quantification of metastatic lung nodules. Data are presented as mean ± SD from three independent experiments. Control: parental A498 cells; Vector: A498 cells transduced with control lentivirus; DCST1-AS1: A498 cells expressing DCST1-AS1 lentivirus. $p < 0.05$; **p** < 0.01; **p** < 0.001 (Student's t-test or one-way ANOVA).

A lung metastasis model was further employed to evaluate the contribution of DCST1-AS1 to RCC metastatic spread **(Figure 6k)**. Analysis of metastatic burden revealed a significantly higher number of visible metastatic lesions in mice injected with A498 cells stably overexpressing DCST1-AS1, whereas markedly fewer metastatic sites were detected in mice bearing A498/Vector tumors (**Figures 6l–m).** Histopathological examination using H&E staining confirmed the presence of tumor lesions in both primary and lung metastatic tissues. Collectively, these in vivo findings demonstrate that DCST1-AS1 overexpression accelerates RCC tumor growth and promotes metastatic progression.

DCST1-AS1 drives RCC progression through activation of the PI3K/AKT/GSK-3β/β-catenin signaling cascade

To explore the molecular pathways underlying DCST1-AS1–mediated oncogenic effects, KEGG pathway enrichment analysis was conducted using differentially expressed genes identified between DCST1-AS1–overexpressing cells and control cells. This analysis revealed significant enrichment of pathways associated with cell adhesion, cytokine–cytokine receptor interactions, and inflammatory signaling. Notably, the PI3K/AKT pathway emerged as a prominently enriched signaling axis **(Figure 7a).** Consistently, gene set enrichment analysis further demonstrated a strong positive association between DCST1-AS1 expression and PI3K/AKT pathway activation (NES = 1.73, $p < 0.001$, FDR < 0.001; **Figure 7b**). To validate these bioinformatic findings, protein expression analyses were performed in RCC cells following DCST1-AS1 knockdown. Western blot results showed that depletion of DCST1-AS1 markedly decreased the levels of β-catenin, phosphorylated GSK-3β, phosphorylated PI3K, and phosphorylated AKT, while total PI3K and AKT protein levels remained unchanged **(Figures 7c–d).** Similar alterations in signaling components were observed in xenograft tumor tissues derived from DCST1-AS1–overexpressing mice compared with vector controls. Immunofluorescence staining further demonstrated that enforced expression of DCST1-AS1 facilitated the accumulation of β-catenin within the nucleus **(Figure 7e),** suggesting enhanced transcriptional activity of β-catenin–dependent genes. To assess whether PI3K/AKT signaling mediates the pro-tumorigenic effects of DCST1-AS1, cells overexpressing DCST1-AS1 were treated with the PI3K inhibitor LY294002.

Pharmacological inhibition of PI3K/AKT signaling significantly attenuated DCST1-AS1–induced cell proliferation, migration, and invasion. Taken together, these results indicate that DCST1-AS1 promotes RCC progression by activating the PI3K/AKT/GSK-3β pathway and facilitating β-catenin nuclear translocation.

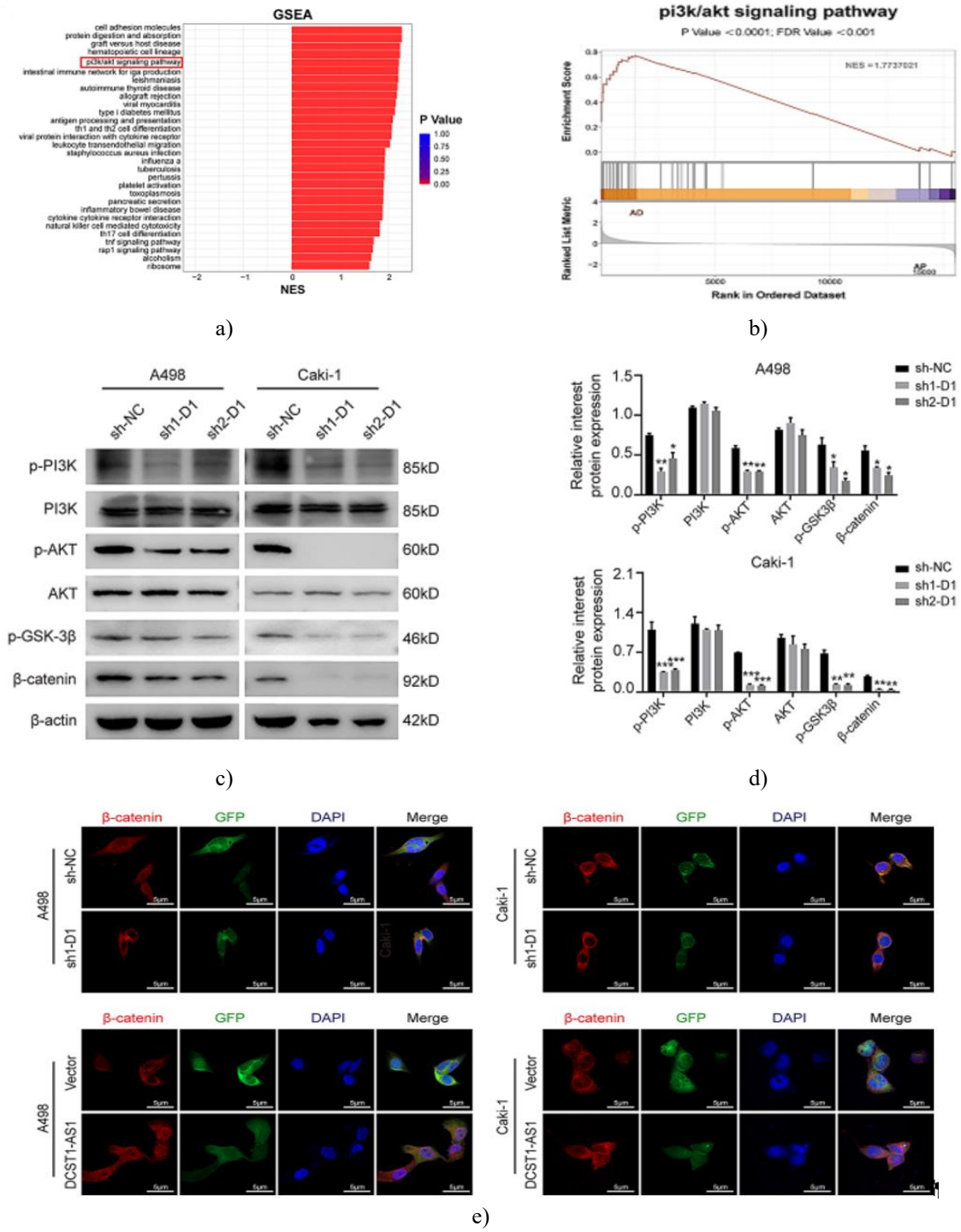

Figure 7. DCST1-AS1 induces activation of the PI3K/AKT/GSK-3β signaling cascade. a**.** KEGG pathway enrichment analysis of differentially expressed genes in A498 cells with enforced DCST1-AS1 expression; NES

denotes normalized enrichment score. b**.** Gene set enrichment analysis demonstrating a significant association between DCST1-AS1 overexpression and PI3K/AKT pathway activation. c, d**.** Immunoblot analyses assessing total and phosphorylated forms of PI3K and AKT, as well as phospho-GSK-3β and β-catenin, in DCST1-AS1–overexpressing RCC cells. e**.** Immunofluorescence staining showing intracellular distribution of β-catenin (red) following DCST1-AS1 overexpression. Scale bar = 5 μm. Data are presented as mean ± SD from three independent experiments. $p < 0.05$; **p** < 0.01; **p** < 0.001 (Student's t-test or one-way ANOVA).

Advances in transcriptome sequencing have led to the identification of a rapidly expanding number of long noncoding RNAs (lncRNAs), many of which have been shown to play regulatory roles in cancer development and progression [4, 11, 29]. Beyond well-studied lncRNAs, continued exploration of previously uncharacterized lncRNAs may provide important insights into the molecular mechanisms underlying renal cell carcinoma (RCC). In this study, we analyzed RNA-sequencing datasets derived from RCC patients to screen for lncRNAs exhibiting differential expression between tumor and normal kidney tissues. Through this approach, we identified DCST1-AS1 as a novel lncRNA of interest. DCST1-AS1 has previously been reported to be upregulated in several malignancies, including endometrial cancer [17], oral squamous cell carcinoma [30], glioblastoma [31], and breast cancer [32]. Our data demonstrated that DCST1-AS1 expression was markedly elevated in RCC tissues and cell lines and was positively associated with aggressive clinicopathological features, such as higher tumor grade, advanced TNM stage, increased histological grade, and unfavorable patient outcomes. Survival analyses further revealed that elevated DCST1-AS1 expression correlated with reduced overall survival (OS), progression-free interval (PFI), and disease-free survival (DFS) in RCC patients. Multivariate Cox regression analysis confirmed that DCST1-AS1 served as an independent predictor of poor OS. Collectively, these findings suggest that DCST1-AS1 may represent a promising prognostic biomarker for RCC, although it should be noted that these clinical correlations were derived from publicly available datasets.

Previous studies have shown that suppression of DCST1-AS1 inhibits tumor cell proliferation in several cancer types [33–35]; however, its biological function in RCC had not been previously elucidated. Our loss-of-function experiments demonstrated that silencing DCST1-AS1 significantly impaired RCC cell proliferation and clonogenic capacity and induced cell cycle arrest. In contrast, enforced expression of DCST1-AS1 markedly enhanced tumor growth and metastatic potential in xenograft mouse models. Mechanistically, DCST1-AS1 knockdown resulted in G1/S phase arrest, accompanied by reduced expression of key cell cycle regulators, including CDK2, CDK4, and Cyclin D1. These observations are consistent with a recent report showing that DCST1-AS1 depletion suppresses hepatocellular carcinoma cell proliferation by inducing G1/S arrest [18]. Given the well-established association between metastasis and cancer-related mortality [36], we further evaluated the role of DCST1-AS1 in RCC cell dissemination. Loss of DCST1-AS1 significantly attenuated RCC cell migration and invasion in vitro, whereas its overexpression increased the number of detectable metastatic lymph nodes in a lung metastasis model. DCST1-AS1 has also been reported to promote TGF-β–induced epithelial–mesenchymal transition (EMT) through regulation of ANXA1 in breast cancer cells [37]. EMT is characterized by the loss of epithelial polarity and acquisition of mesenchymal traits [38]. Consistent with this process, DCST1-AS1 knockdown in RCC cells led to increased expression of the epithelial marker E-cadherin and decreased levels of mesenchymal markers, including vimentin and N-cadherin. Together, these findings indicate that DCST1-AS1 functions as an oncogenic lncRNA that facilitates RCC initiation and progression.

Accumulating evidence suggests that DCST1-AS1 can act as a competing endogenous RNA (ceRNA), sequestering microRNAs to regulate downstream gene expression [39–41]. In the present study, DCST1-AS1 was predominantly localized in the cytoplasm of RCC cells, supporting its potential role in miRNA-mediated post-transcriptional regulation. Analysis of starBase datasets revealed a significant inverse correlation between DCST1-AS1 and miR-582-5p expression in RCC tissues. miR-582-5p has previously been characterized as a tumor suppressor in multiple malignancies [25, 42, 43], and reduced miR-582-5p expression has been associated with advanced tumor stage and metastatic disease in clear cell RCC [44], highlighting its potential prognostic relevance. Our results showed that miR-582-5p expression exhibited an

opposing pattern to that of DCST1-AS1 in RCC. Moreover, restoration of miR-582-5p partially rescued the inhibitory effects induced by DCST1-AS1 knockdown. Subsequent luciferase reporter and RNA pull-down assays confirmed that DCST1-AS1 directly binds miR-582-5p, thereby functioning as a molecular sponge in RCC cells.

HMGB2, a non-histone chromatin-associated protein [45], plays important roles in diverse biological processes, including cellular aging, lipid metabolism, and immune and inflammatory responses [46, 47]. Aberrant upregulation of HMGB2 has been reported in various solid tumors [26, 48]. Notably, a recent study by He *et al*. demonstrated that HMGB2 expression is elevated in renal tumors and correlates with poor overall survival in RCC patients [27]. In this study, we identified HMGB2 as a direct downstream target of miR-582-5p in RCC cells. Correlation analyses further showed that RCC tissues with high DCST1-AS1 expression displayed concomitant downregulation of miR-582-5p and upregulation of HMGB2. Functional rescue experiments revealed that reintroduction of HMGB2 restored the malignant phenotypes suppressed by DCST1-AS1 knockdown, indicating that DCST1-AS1 promotes RCC progression through a regulatory DCST1-AS1/miR-582-5p/HMGB2 axis.

Dysregulation of the PI3K/AKT/GSK-3β signaling pathway has been widely implicated in tumor-associated processes, including cell proliferation, migration, angiogenesis, apoptosis, and autophagy [49–51]. Our pathway enrichment analyses, together with extensive experimental validation, demonstrated that DCST1-AS1 enhances RCC progression by activating the PI3K/AKT/GSK-3β cascade and promoting nuclear translocation of β-catenin. Stabilization and accumulation of β-catenin require modulation of GSK-3β activity [52]. Specifically, phosphorylation of GSK-3β at Ser9 by activated AKT leads to GSK-3β inactivation, thereby preventing cytoplasmic β-catenin degradation [53, 54]. Once translocated to the nucleus, β-catenin activates TCF/LEF transcription factors, ultimately regulating genes involved in cell adhesion and cell cycle progression [55]. One limitation of the present study is the lack of validation of the ceRNA regulatory network and the DCST1-AS1–β-catenin relationship in a larger cohort of human RCC specimens. Future studies are therefore warranted to further explore the clinical relevance of DCST1-AS1 and to assess its potential utility as a biomarker or therapeutic target across different cancer types.

Conclusion

In summary, this study establishes DCST1-AS1 as a key oncogenic lncRNA in RCC. Its expression is significantly elevated in RCC tissues and correlates with poor patient prognosis. Functional experiments demonstrated that DCST1-AS1 drives tumor growth and metastasis in both in vitro and in vivo models. Mechanistically, DCST1-AS1 acts as a molecular sponge for miR-582-5p, leading to increased HMGB2 expression, and promotes RCC progression through activation of the PI3K/AKT/GSK-3β signaling pathway. These findings highlight DCST1-AS1 as a potential therapeutic target in RCC.

Acknowledgments: None

Conflict of Interest: None

Financial Support: None

Ethics Statement: None

References

1. Rizzo M, Caliò A, Brunelli M, Pezzicoli G, Ganini C, Martignoni G, Camillo P. Clinico-pathological implications of the 2022 WHO renal cell carcinoma classification. Cancer Treat Rev. 2023;116:102558.
2. Capitanio U, Bensalah K, Bex A, Boorjian SA, Bray F, Coleman J, Gore JL, Sun M, Wood C, Russo P. Epidemiology of renal cell carcinoma. Eur Urol. 2019;75:74–84.
3. Linehan WM, Ricketts CJ. The cancer genome atlas of renal cell carcinoma: findings and clinical implications. Nat Reviews Urol. 2019;16:539–52.
4. Loganathan T, Doss CGP. Non-coding RNAs in human health and disease: potential function as biomarkers and therapeutic targets. Funct Integr Genom. 2023;23:33.
5. Mercer TR, Dinger ME, Mattick JS. Long non-coding rnas: insights into functions. Nat Rev Genet. 2009;10:155–9.
6. Herman AB, Tsitsipatis D, Gorospe M. Integrated lncRNA function upon genomic and epigenomic regulation. Mol Cell. 2022;82:2252–66.

7. Han D, Ouyang G, Pan P, Yuan Y. Upregulated lncRNA-NEF predicts recurrence and poor treatment outcomes of ankylosing spondylitis. Immun Inflamm Dis. 2022;10:e627.
8. Zhang Q, Li X, Cui K, Liu C, Wu M, Prochownik EV, Li Y. The MAP3K13-TRIM25-FBXW7α axis affects c-Myc protein stability and tumor development. Cell Death Differ. 2020;27:420–33.
9. Xia A, Yuan W, Wang Q, Xu J, Gu Y, Zhang L, Chen C, Wang Z, Wu D, He Q, et al. The cancer-testis LncRNA lnc-CTHCC promotes hepatocellular carcinogenesis by binding HnRNP K and activating YAP1 transcription. Nat Cancer. 2022;3:203–18.
10. Yang J, Liu F, Wang Y, Qu L, Lin A. LncRNAs in tumor metabolic reprogramming and immune microenvironment remodeling. Cancer Lett. 2022;543:215798.
11. Bridges MC, Daulagala AC, Kourtidis A. LNCcation: lncRNA localization and function. J Cell Biol. 2021:220.
12. Farooqi AA, Attar R, Yulaevna IM, Berardi R. Interaction of long non-coding RNAs and circular RNAs with MicroRNAs for the regulation of immunological responses in human cancers. Semin Cell Dev Biol. 2022;124:63–71.
13. Du L, Wang B, Wu M, Chen W, Wang W, Diao W, Ding M, Chen W, Cao W, Guo H, Zhang G. LINC00926 promotes progression of renal cell carcinoma via regulating miR-30a-5p/SOX4 axis and activating IFNγ-JAK2-STAT1 pathway. Cancer Lett. 2023;578:216463.
14. Wang J, Zou Y, Du B, Li W, Yu G, Li L, Zhou L, Gu X, Song S, Liu Y, et al. SNP-mediated lncRNA-ENTPD3-AS1 upregulation suppresses renal cell carcinoma via miR-155/HIF-1α signaling. Cell Death Dis. 2021;12:672.
15. Su YZ, Cui MF, Du J, Song B. LncRNA DCST1-AS1 regulated cell proliferation, migration, invasion and apoptosis in gastric cancer by targeting miR-605-3p. Eur Rev Med Pharmacol Sci. 2021;25:6827.
16. Wang J, Shi P, Teng H, Lu L, Guo H, Wang X. Corrigendum: LncRNA DCST1-AS1 promotes endometrial cancer progression by modulating the MiR- 665/HOXB5 and MiR-873-5p/CADM1 pathways. Front Oncol. 2022;12:819908.
17. Ke J, Shen Z, Hu W, Li M, Shi Y, Xie Z, Wu D. LncRNA DCST1-AS1 was upregulated in endometrial carcinoma and May sponge miR-92a-3p to upregulate Notch1. Cancer Manage Res. 2020;12:1221–7.
18. Chen J, Wu D, Zhang Y, Yang Y, Duan Y, An Y. LncRNA DCST1-AS1 functions as a competing endogenous RNA to regulate FAIM2 expression by sponging miR-1254 in hepatocellular carcinoma. Clin Sci (London England: 1979). 2019;133:367–79.
19. Pokorná M, Černá M, Boussios S, Ovsepian SV, O'Leary VB. LncRNA biomarkers of glioblastoma multiforme. Biomedicines. 2024:12.
20. Liang C, Wang J, Liu A, Wu Y. Tumor promoting long non-coding RNA CASC15 affects HMGB2 expression by sponging miR-582-5p in colorectal cancer. J Gene Med. 2022;24:e3308.
21. Wang F, Luo Y, Zhang L, Younis M, Yuan L. The LncRNA RP11-301G19.1/miR-582-5p/HMGB2 axis modulates the proliferation and apoptosis of multiple myeloma cancer cells via the PI3K/AKT signalling pathway. Cancer Gene Ther. 2021;29:292–303.
22. Zhao Y, Li Y, Su M, Cai X. Predictive value of miR-582-5p for onset of sepsis-induced acute kidney injury and its functional role during disease development. Central-European J Immunol. 2024;49:383–92.
23. Du X, Luo W, Li H, Gu Q, Huang P, Wang C, Li N, Liu F, Xia C. Hsa_circ_0125356 promotes gemcitabine resistance by modulating WNT canonical and non-canonical pathways via miR-582-5p/FGF9 axis in non-small cell lung cancer. Mol Cancer. 2025;24:59.
24. Chen F, Guo L, Di J, Li M, Dong D, Pei D. Circular RNA ubiquitin-associated protein 2 enhances autophagy and promotes colorectal cancer progression and metastasis via miR-582-5p/FOXO1 signaling. J Genet Genomics = Yi Chuan Xue Bao. 2021;48:1091–103.
25. Huang S, Zou C, Tang Y, Wa Q, Peng X, Chen X, Yang C, Ren D, Huang Y, Liao Z et al. miR-582-3p and miR-582-5p suppress prostate cancer metastasis to bone by repressing TGF-β signaling. Mol Therapy Nucleic Acids. 2019:16.
26. Starkova T, Polyanichko A, Tomilin AN, Chikhirzhina E. Structure and functions of HMGB2 protein. Int J Mol Sci. 2023:24.
27. He ZH, Guo F, Hu XX, Luo ZY, Yi JW. Knockdown of HMGB2 inhibits proliferation and invasion of

renal tumor cells via the p-38MAPK pathway. Eur Rev Med Pharmacol Sci. 2020;24:4729–37.
28. Hu J, Dai C, Ding Z, Pan Y, Lu L, Bao J, Zheng J. IKBIP promotes tumor development via the Akt signaling pathway in esophageal squamous cell carcinoma. BMC Cancer. 2024;24:759.
29. Chen L-L, Kim VN. Small and long non-coding rnas: Past, present, and future. Cell. 2024;187:6451–85.
30. Ai Y, Liu S, Luo H, Wu S, Wei H, Tang Z, Li X, Zou C. LncRNA DCST1-AS1 facilitates oral squamous cell carcinoma by promoting M2 macrophage polarization through activating NF-κB signaling. J Immunol Res. 2021;2021:5524231.
31. Hu S, Yao Y, Hu X, Zhu Y. LncRNA DCST1-AS1 downregulates miR-29b through methylation in glioblastoma (GBM) to promote cancer cell proliferation. Clin Translational Oncology: Official Publication Federation Span Oncol Soc Natl Cancer Inst Mexico. 2020;22:2230–5.
32. Tang L, Chen Y, Tang X, Wei D, Xu X, Yan F. Long noncoding RNA DCST1-AS1 promotes cell proliferation and metastasis in Triple-negative breast cancer by forming a positive regulatory loop with miR-873-5p and MYC. J Cancer. 2020;11:311–23.
33. Liu J, Zhang J, Hu Y, Zou H, Zhang X, Hu X. Inhibition of LncRNA DCST1-AS1 suppresses proliferation, migration and invasion of cervical cancer cells by increasing miR-874-3p expression. J Gene Med. 2021;23:e3281.
34. Zhou Z, Xia N. LncRNA DCST1-AS1 sponges miR-107 to upregulate CDK6 in cervical squamous cell carcinoma. Cancer Manage Res. 2020;12:7921–8.
35. Li J, Zhai DS, Huang Q, Chen HL, Zhang Z, Tan QF. LncRNA DCST1-AS1 accelerates the proliferation, metastasis and autophagy of hepatocellular carcinoma cell by AKT/mTOR signaling pathways. Eur Rev Med Pharmacol Sci. 2019;23:6091–104.
36. Cho BC, Felip E, Hayashi H, Thomas M, Lu S, Besse B, Sun T, Martinez M, Sethi SN, Shreeve SM, Spira AI. MARIPOSA: phase 3 study of first-line amivantamab + lazertinib versus osimertinib in EGFR-mutant non-small-cell lung cancer. Future Oncol (London England). 2022;18:639–47.
37. Tang L, Chen Y, Chen H, Jiang P, Yan L, Mo D, Tang X, Yan F. DCST1-AS1 promotes TGF-β-Induced Epithelial-Mesenchymal transition and enhances chemoresistance in Triple-Negative breast cancer cells via ANXA1. Front Oncol. 2020;10:280.
38. Bischoff J. Endothelial-to-Mesenchymal transition. Circul Res. 2019;124:1163–5.
39. Wu X, Sui Z, Zhang H, Wang Y, Yu Z. Integrated analysis of lncRNA-Mediated CeRNA network in lung adenocarcinoma. Front Oncol. 2020;10:554759.
40. Zhang C, Yu Z, Yang S, Liu Y, Song J, Mao J, Li M, Zhao Y. ZNF460-mediated circRPPH1 promotes TNBC progression through ITGA5-induced FAK/PI3K/AKT activation in a CeRNA manner. Mol Cancer. 2024;23:33.
41. Braga EA, Fridman MV, Moscovtsev AA, Filippova EA, Dmitriev AA, Kushlinskii NE. LncRNAs in ovarian cancer progression, metastasis, and main pathways: ceRNA and alternative mechanisms. Int J Mol Sci. 2020:21.
42. Hu Y, Su Y, Lei X, Zhao H, Wang L, Xu T, Guo J, Yang W, Zhang X. LINC00641/miR-582-5p mediate oxaliplatin resistance by activating autophagy in gastric adenocarcinoma. Sci Rep. 2020;10:14981.
43. Tian Y, Guan Y, Su Y, Luo W, Yang G, Zhang Y. MiR-582-5p inhibits bladder Cancer-Genesis by suppressing TTK expression. Cancer Manage Res. 2020;12:11933–44.
44. Xue J, Zhu S, Qi F, Zhu K, Cao P, Yang J, Wang Z. RUNX1/miR-582-5p pathway regulates the tumor progression in clear cell renal cell carcinoma by targeting COL5A1. Front Oncol. 2021;11:610992.
45. Kong D, Liu J, Lu J, Zeng C, Chen H, Duan Z, Yu K, Zheng X, Zou P, Zhou L, et al. HMGB2 release promotes pulmonary hypertension and predicts severity and mortality of patients with pulmonary arterial hypertension. Arterioscler Thromb Vasc Biol. 2024;44:e172–95.
46. Qu W-F, Zhu G-Q, Yang R, Chu T-H, Guan Z-Q, Huang R, Tian M-X, Jiang X-F, Tao C-Y, Fang Y, et al. Targeting HMGB2 acts as dual Immunomodulator by bolstering CD8 + T cell function and inhibiting tumor growth in hepatocellular carcinoma. Sci Adv. 2025;11:eads8597.
47. Starkova TY, Polyanichko AM, Artamonova TO, Tsimokha AS, Tomilin AN, Chikhirzhina EV. Structural characteristics of high-mobility group proteins HMGB1 and HMGB2 and their interaction with DNA. Int J Mol Sci. 2023:24.
48. Chen Y-Z, Meng Z-S, Xiang Z-L. HMGB2 drives tumor progression and shapes the

immunosuppressive microenvironment in hepatocellular carcinoma: insights from multi-omics analysis. Front Immunol. 2024;15:1415435.

49. Guo Z, Li Z, Guo J, Gan L, Mo H, Zhang J, Fu Y, Wang Y, Jin M, Wu Y, et al. A N7-methylguanosine modified circular RNA, circIPP2A2, promotes malignant behaviors in hepatocellular carcinoma by serving as a scaffold in modulating the Hornerin/PI3K/AKT/GSK3β axis. Cell Death Dis. 2024;15:868.
50. Liang S, Guo H, Ma K, Li X, Wu D, Wang Y, Wang W, Zhang S, Cui Y, Liu Y, et al. A PLCB1-PI3K-AKT signaling axis activates EMT to promote cholangiocarcinoma progression. Cancer Res. 2021;81:5889–903.
51. Zhao S-J, Kong F-Q, Jie J, Li Q, Liu H, Xu A-D, Yang Y-Q, Jiang B, Wang D-D, Zhou Z-Q, et al. Macrophage MSR1 promotes BMSC osteogenic differentiation and M2-like polarization by activating PI3K/AKT/GSK3β/β-catenin pathway. Theranostics. 2020;10:17–35.
52. Franke TF, Hornik CP, Segev L, Shostak GA, Sugimoto C. PI3K/Akt and apoptosis: size matters. Oncogene. 2003;22:8983–98.
53. Li J, Xuan W, Yan R, Tropak MB, Jean-St-Michel E, Liang W, Gladstone R, Backx PH, Kharbanda RK, Redington AN. Remote preconditioning provides potent cardioprotection via PI3K/Akt activation and is associated with nuclear accumulation of β-catenin. Clin Sci (London England: 1979). 2011;120:451–62.
54. Jiang H, Zhou Z, Jin S, Xu K, Zhang H, Xu J, Sun Q, Wang J, Xu J. PRMT9 promotes hepatocellular carcinoma invasion and metastasis via activating PI3K/Akt/GSK-3β/Snail signaling. Cancer Sci. 2018;109:1414–27.
55. Liu J, Xiao Q, Xiao J, Niu C, Li Y, Zhang X, Zhou Z, Shu G, Yin G. Wnt/β-catenin signalling: function, biological mechanisms, and therapeutic opportunities. Signal Transduct Target Therapy. 2022;7:3.